

Radio Crickets: Chirping Jets from Black Hole Binaries Entering their Gravitational Wave Inspiral

Girish Kulkarni^{1*} and Abraham Loeb^{2†}

¹*Institute of Astronomy and Kavli Institute of Cosmology, University of Cambridge, Madingley Road, Cambridge CB3 0HA, UK*

²*Institute for Theory & Computation, Harvard University, 60 Garden Street, Cambridge, MA 02138, USA*

Accepted —. Received —; in original form —

ABSTRACT

We study a novel electromagnetic signature of supermassive black hole binaries whose inspiral starts being dominated by gravitational wave (GW) emission. Recent simulations suggest that the binary’s member BHs can continue to accrete gas from the circumbinary accretion disk in this phase of the binary’s evolution, all the way until coalescence. If one of the binary members produces a radio jet as a result of accretion, the jet precesses along a biconical surface due to the binary’s orbital motion. When the binary enters the GW phase of its evolution, the opening angle widens, the jet exhibits milliarcsecond scale wiggles, and the conical surface of jet precession is twisted due to apparent superluminal motion. The rapidly increasing orbital velocity of the binary gives the jet an appearance of a “chirp.” This helical chirping morphology of the jet can be used to infer the binary parameters. For binaries with mass 10^7 – 10^{10} M_{\odot} at redshifts $z < 0.5$, monitoring these features in current and archival data will place a lower limit on sources that could be detected by eLISA and Pulsar Timing Arrays. In the future, microarcsecond interferometry with the Square Kilometer Array will increase the potential usefulness of this technique.

Key words: accretion, accretion discs – black hole physics – quasars: supermassive black holes

1 INTRODUCTION

Binaries of supermassive black holes (BHs) arise naturally as a result of mergers of galaxies in the context of hierarchical galaxy formation (Kauffmann & Haehnelt 2000; Haehnelt & Kauffmann 2002; Di Matteo et al. 2008; Kulkarni & Loeb 2012). After a galaxy merger, infalling black holes lose their angular momentum in three stages before coalescence (Begelman et al. 1980; Merritt & Milosavljević 2005; Colpi & Dotti 2011). In the first stage, the black holes sink to the center of the gravitational potential of the merger remnant due to dynamical friction and form a gravitationally bound binary. The newly formed binary then continues to lose its angular momentum and shrink by scattering ambient gas and stars. In the final stage of the binary’s evolution, emission of gravitational waves (GWs) becomes the predominant mode of angular momentum loss, which results in the coalescence of the black holes.

General relativistic (GR) numerical simulations can predict the binary’s evolution in its final stage up to coalescence

(Pretorius 2005; Baker et al. 2006; Campanelli et al. 2006). This has stimulated interest in predicting related electromagnetic signals of black hole coalescence. Effects considered in the literature include afterglows due to infall of gas on the remnant black hole (Milosavljević & Phinney 2005), electromagnetic variability in the circumbinary disk due to shocks induced by the sudden mass loss of the binary following GW emission at coalescence (Bode & Phinney 2007; Lippai et al. 2008), flares from shocked remnants of accretion disk around the recoiled remnant black hole (Loeb 2007; Shields & Bonning 2008; Haiman et al. 2009), quasi-periodic variability in gas accretion in the early stages of black hole merger (MacFadyen & Milosavljević 2008; Haiman et al. 2009; Kocsis et al. 2012; D’Orazio et al. 2013; Farris et al. 2014; Shi & Krolik 2015), evolution in the profiles of broad emission lines shortly before merger (McKernan et al. 2013), characteristic evolution in thermal emission due to circumbinary accretion (Farris et al. 2015), brightening of the circumbinary accretion disk due to viscous dissipation of gravitational waves (Kocsis & Loeb 2008), and prompt tidal disruption of ambient stars by the recoiled remnant (Stone & Loeb 2011).

In addition to testing GR in the strong field limit, observations of electromagnetic counterparts will help localize

* E-mail: kulkarni@ast.cam.ac.uk

† E-mail: aloeb@cfa.harvard.edu

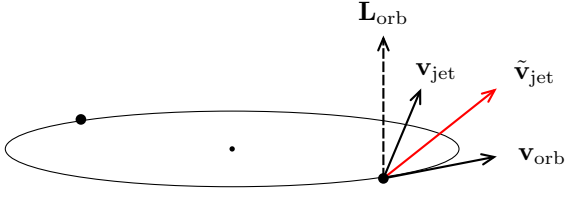


Figure 1. Jet and orbital configuration. The orbital velocity \mathbf{v}_{orb} causes the jet to precess as its source BH moves along its binary orbit. The net jet velocity is $\tilde{\mathbf{v}}_{\text{jet}} = \mathbf{v}_{\text{orb}} + \mathbf{v}_{\text{jet}}$, where \mathbf{v}_{jet} is its ejection velocity of the jet material at the source.

sources of GWs for future detectors such as the Evolved Laser Interferometer Space Antenna (eLISA)¹, which would be capable of observing the peak GW luminosity for BH coalescence of $\sim 10^{57}$ erg/s out to cosmological distances (Hughes & Holz 2003; Sesana 2013). Simultaneous detection of GW and electromagnetic signals from coalescing binaries will yield rich scientific pay-offs (Hughes & Holz 2003; Holz & Hughes 2005). For example, redshift measurement of eLISA sources could constraint cosmological parameters. Measurement of the black hole masses and spins from the GW signal could constrain accretion physics during coalescence. But even before eLISA is launched, a search of electromagnetic signatures may help calibrate the expected abundance of GW sources.

In this paper, we study the morphology of jets from binary BHs whose dynamics is dominated by GW emission. Jets in binary BHs have been studied in a number of previous works (Sarazin et al. 1980; Icke 1981; Hjellming & Johnston 1981; Gower & Hutchings 1982b,a; Gower et al. 1982). It has been shown that the orbital motion of binary results in a precession of the jet, resulting in a helical or “wiggly” jet morphology. Such models of jet precession have been used to understand the observed jet morphology in several AGN. For example, recently Kun et al. (2014) fit a jet precession model to the observed jet in the quasar S5 1928+738 using 18 yr of very long baseline interferometric (VLBI) data. This object was first studied using BH binary models by Roos et al. (1993), but Kun et al. (2014) also included effects of BH spin. Other objects studied in this manner are PG 1302-102 (Kun et al. 2015; Graham et al. 2015b), BL Lacertae (Stirling et al. 2003; Caproni et al. 2013), NGC 4151 (Bon et al. 2012), OJ 287 (Valtonen & Wiik 2012), S5 1803+784 (Roland et al. 2008), 3C 345 (Lobanov & Roland 2005), 3C 210 (Caproni & Abraham 2004), PKS 420-014 (Britzen et al. 2001), 3C 273 (Romero et al. 2000), and Mrk 501 (Villata & Raiteri 1999). Gower et al. (1982) also studied several AGN using their model of jet precession.

The shortest binary separations inferred from these studies are of the order of 10^{-2} pc. At smaller separations of around 10^{-3} pc, the orbital velocity of the BHs typically becomes relativistic ($v_{\text{orb}} \sim 10^4$ km/s or $\beta \sim 0.01$). It was thought that at these small separations, the binary evolves in a vacuum, because the inspiral time scale of the binary is likely shorter than the viscous time scale of any circumbinary gas disk. As a result, gas fails to catch up with the BHs, making any accretion activity impossible in

this stage of the binary’s evolution (Milosavljević & Phinney 2005; Shapiro 2010; Tanaka & Menou 2010). However recent viscous hydrodynamical simulations do not find this decoupling between the BHs and the circumbinary disk. In these simulations, the binary’s member BHs can continue to accrete gas from the circumbinary accretion disk all the way until coalescence (Farris et al. 2012; D’Orazio et al. 2013; Gold et al. 2014a,b; Farris et al. 2015; Shi & Krolik 2015). This opens up the possibility of jet production by one of the binary members during the binary’s final phase of evolution before coalescence, i.e., when the binary’s dynamics is dominated by GW emission. In this paper we study the morphology of such jets.

All of the above models of jet precession in binary BHs consider stable binaries, in which the time scale of evolution of the binary separation is much larger than the orbital period of the binary. For such binaries, the helical morphology of the jet is does not change significantly between precession cycles. However, we will see below that for a binary BH with separation a , the orbital period is proportional to $a^{1.5}$, while the time scale of evolution of the binary separation is proportional to a^4 . Thus, as the binary shrinks, the latter time scale decreases much more rapidly than the former, and for small enough separations, the two time scales can be comparable. In this paper, we study jets in this previously ignored regime. We show that at this stage of the binary’s evolution, the jet morphology is more complicated: the jet now has a peculiar helical chirping morphology. We further argue that in this case the jet morphology can be used to infer the binary parameters and show how such features can be distinguished from the usual helical jet morphology.

2 BINARY PARAMETERS

We study a BH binary formed following a gas-rich merger of two galaxies as a result of the processes described above. We consider black holes with masses M_1 and M_2 in a circular orbit of radius a around each other. Let $M = M_1 + M_2$. For simplicity, we consider an equal-mass binary ($M_1 = M_2$) on a circular orbit. The orbital speed of each black hole is given by

$$v_{\text{orb}} = \frac{1}{2} \left(\frac{GM}{a} \right)^{1/2} = 5.8 \times 10^3 \text{ km s}^{-1} M_8^{1/2} a_{16}^{-1/2}, \quad (1)$$

where $a_{16} \equiv (a/10^{16} \text{ cm})$ and $M_8 \equiv (M/10^8 M_\odot)$ are the binary separation and mass, respectively.² The orbital period is

$$P = 2\pi \left(\frac{GM}{a^3} \right)^{-1/2} = 1.72 \text{ yr } a_{16}^{3/2} M_8^{-1/2}. \quad (2)$$

In a gas-rich galaxy merger, the BH binary loses its angular momentum by torquing the surrounding disk through spiral arms and expelling gas out of a region twice as large as the binary orbit (Artymowicz & Lubow 1994; Milosavljević & Phinney 2005; Hayasaki et al. 2007; MacFadyen & Milosavljević 2008; Cuadra et al. 2009). The expelled gas carries a specific angular momentum of $\sim va$. Further angular momentum dissipation of the binary can happen due

¹ <https://www.elisascience.org>

² Note that $10^{16} \text{ cm} \approx 3.4 \times 10^{-3} \text{ pc}$. The Schwarzschild radius of a $10^8 M_\odot$ black hole is $9.6 \times 10^{-6} \text{ pc}$, or $\sim 3 \times 10^{13} \text{ cm}$.

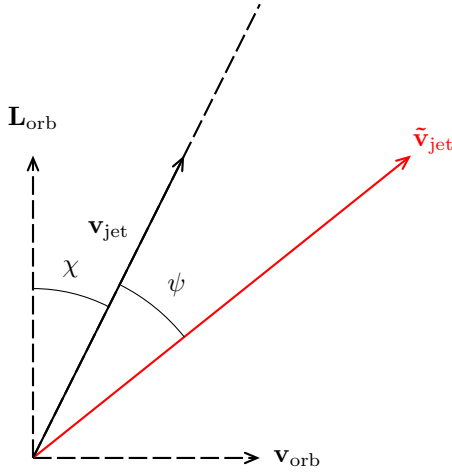


Figure 2. The orbital velocity \mathbf{v}_{orb} introduces the jet precession angle ψ . Without the orbital motion, $\psi = 0$, and the jet traces a cylindrical surface. With the orbital motion, the net red velocity vector oscillates around the solid black vector and produces a conical surface with ψ as its half-opening angle. Note that v_{orb} is exaggerated here. In practice, $v_{\text{orb}} \ll v_{\text{jet}} \sim c$. The figure indicates that $\sin \psi \sim \tan \psi = v_{\text{orb}} \cos \chi / v_{\text{jet}}$.

to its interaction with fresh gas that enters the hollowed out region as a result of tidal torques (MacFadyen & Milosavljević 2008; Noble et al. 2012; Kocsis et al. 2012; Roedig et al. 2012). Therefore, the coalescence time of the binary is inversely proportional to the rate at which fresh gas re-enters the binary region. But only a fraction of gas that enters the central hollow region accretes onto the black hole and fuels quasar activity. Therefore, we express \dot{M} in Eddington units, $\dot{\mathcal{M}} \equiv \dot{M}/\dot{M}_E$, where \dot{M}_E is the accretion rate required to power the limiting Eddington luminosity with a radiative efficiency of 10%, $\dot{M}_E = 2.3M_{\odot} \text{ yr}^{-1} M_8$. We therefore have (Loeb 2010; Dotti et al. 2015)

$$\frac{a}{\dot{a}} = t_{\text{gas}} \approx \frac{J}{\dot{M} v a} = 1.1 \times 10^7 \text{ yr } \dot{\mathcal{M}}^{-1}, \quad (3)$$

where $J = \mu v a$ is the binary’s angular momentum and $\mu = M/2$ is the binary’s reduced mass. This time scale is greater by two orders of magnitude than the time scale for coalescence due to angular momentum loss by GW emission, which for circular orbits is given by (Peters 1964)

$$\frac{a}{\dot{a}} = t_{\text{GW}} = \frac{5}{256} \frac{c^5 a^4}{G^3 M^2 \mu} = 2.53 \times 10^5 \text{ yr } \frac{a_{16}^4}{M_8^3}. \quad (4)$$

By setting $t_{\text{gas}} = t_{\text{GW}}$, we can get the orbital parameters for the binary when GWs take over. The orbital speed at this stage of the binary’s evolution is given by

$$v_{\text{orb}} = 3.6 \times 10^3 \text{ km s}^{-1} (\dot{\mathcal{M}} M_8)^{1/8}, \quad (5)$$

The separation between the two black holes at this instant is given by

$$a = 8.3 \times 10^{-3} \text{ pc } M_8^{3/4} \dot{\mathcal{M}}^{-1/4}. \quad (6)$$

Note that the separation is dependent on the gas accretion rate.

In the GW dominated phase of binary’s evolution, recent simulations show that the BHs can continue to accrete gas from the circumbinary disk all the way until merger

(Farris et al. 2015). At this stage, we consider a ballistic jet emanating from one of binary’s member BHs at speed $\beta = v_{\text{jet}}/c$ at an angle χ to the direction of the orbital angular momentum. This geometry is depicted in Figures 1 and 2. As a result of the binary orbit, the jet will wiggle on a conical surface. (In the limit of a small binary velocity, i.e., at large relative separations, the jet material will move on a cylindrical surface.) The half-opening angle of the cone is given by (Roos et al. 1993)

$$\sin \psi = \frac{v_{\text{orb}} \cos \chi}{v_{\text{jet}}}. \quad (7)$$

(Note that this relation is valid in the $v_{\text{orb}} \ll v_{\text{jet}} \sim c$. Also, we are ignoring any relativistic corrections to this equation.)

When the binary separation reaches the point where gravitational wave-induced inspiral begins, the binary has a velocity given by equation (5), and a separation given by equation (6). From equation (1), the orbital velocity of each BH evolves as

$$\frac{\dot{v}_{\text{orb}}}{v_{\text{orb}}} = -\frac{1}{2} \frac{\dot{a}}{a}. \quad (8)$$

which gives the evolution of the opening angle of the cone as

$$\dot{\psi} = -\frac{1}{2} \frac{\dot{a}}{\cot \psi a}. \quad (9)$$

This can be solved analytically to get

$$\sin \psi = \sin \psi_0 \left(\frac{a_0}{a} \right)^{1/2}, \quad (10)$$

where ψ_0 and a_0 are the initial values. Thus, as the binary continues to shrink the BH orbital velocity grows and the opening angle of the conical jet increases (cone opens wider). The rate at which this happens reflects the binary’s dynamical evolution.

3 JET PRECESSION

We now ask if it would be possible to observe the opening of the jet morphology. For this purpose, it is necessary to map the above calculations to the observer’s frame (Gower et al. 1982). At a large distance compared to the binary’s separation, the jet geometry is illustrated in Figure 3. Here the source frame of reference is shown by x', y', z' coordinate systems. The x, y, z coordinate system represents the observer’s frame such that the yz is the plane of the sky. Further, the jet is oriented such that the y' axis coincides with the y axis, the original direction of jet emission is at an angle i relative to the line of sight (x -axis). For simplicity, we also assume that the z' axis is in the xz plane. Then the jet will precess on a cone with a half-opening angle ψ and an angular velocity of precession Ω . In the source frame of reference, the equation of the jet is then given by (Hjellming & Johnston 1981)

$$v_x = s_{\text{jet}} \beta c [\sin \psi \sin i \cos \Omega t + \cos \psi \cos i], \quad (11)$$

$$v_y = s_{\text{jet}} \beta c \sin \psi \sin \Omega t, \quad \text{and} \quad (12)$$

$$v_z = s_{\text{jet}} \beta c [\cos \psi \sin i - \sin \psi \cos i \cos \Omega t]. \quad (13)$$

Here $s_{\text{jet}} = \pm 1$ for forward and backward jets, respectively. The coordinates of a jet particle in the sky is then given

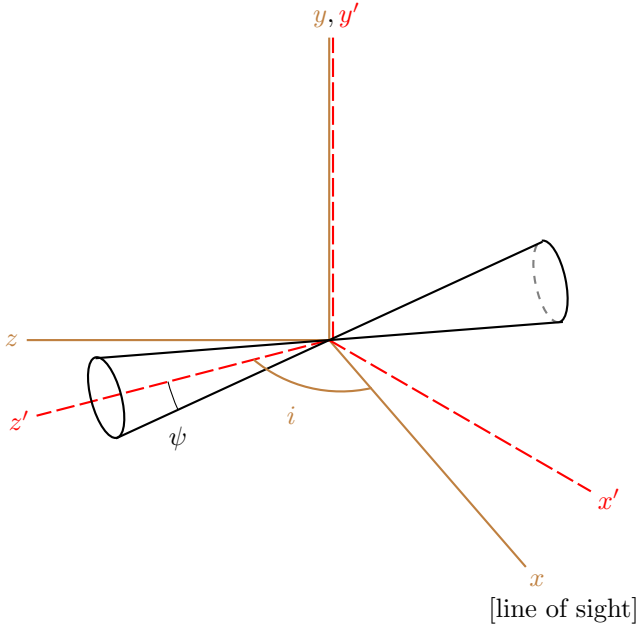


Figure 3. Geometry of the jet (Gower et al. 1982). The observer’s sky is in the yz plane, so that the line of sight is along the x -axis. The jet precesses around the z' axis with half-opening angle ψ . The y and y' axes overlap, and z , x , and z' axes are co-planer. The angle between the z' axis and the line of sight is i . This geometry is valid in the limit $a \ll z'\psi$.

by $z = v_z t$ and $y = v_y t$. However, because of superluminal motion, the observer will see this on the sky as

$$z = v_z t / (1 - v_x/c) \quad (14)$$

and

$$y = v_y t / (1 - v_x/c) \quad (15)$$

respectively. In angular coordinates, the motion of the jet on the sky is given by $\phi_z = z/d$ and $\phi_y = y/d$ where d is the angular diameter distance of the binary. Because of superluminal motion, the forward jet is stretched while the backward jet is compressed.

Finally, we assume that the emission from each jet is optically thin at the frequency of observation with a spectrum in the rest frame of the particle given by $P(\nu) \propto \nu^{-\alpha}$ (Gower et al. 1982). The observed flux density $S(\nu)$ in $\text{erg cm}^{-2} \text{Hz}^{-1}$ is given by

$$S(\nu) = S_r(\nu) D^{3+\alpha}, \quad (16)$$

where D is the Doppler shift parameter $[\gamma(1 - \beta \cos \phi)]^{-1}$ and S_r is the rest frame flux density. Further, to consider the effects of jet evolution we assume that S_r decreases with time according to a simple power law

$$S_r \propto t_{\text{proper}}^{-\delta}, \quad (17)$$

where t_{proper} is the proper time in the frame of the jet. We assume $\delta = 1$ and $\alpha = 1$, hereafter (Gower et al. 1982).

4 JET MORPHOLOGY

As the binary evolves, the combination of increasing orbital speed and the apparent superluminal motion effect results

in a jet morphology with an increasing opening angle and increasingly rapid periodic variation, together with a twisted shape. Figure 4 shows these three features for an equal-mass binary with total mass $M = 10^{10} M_\odot$. For concreteness, we have assumed $i = 40^\circ$ and $\beta = 0.9$. The angular diameter distance to the binary is assumed to be $d = 100 \text{ Mpc}$ (which corresponds to redshift $z \sim 0.025$). The forward jet stretches on the sky while the backward jet is compressed due to the apparent superluminal motion. The right panel of Figure 4 zooms into the inner region of the forward jet and shows that the binary creates wiggles in the jet morphology of the order of a milliarcsecond. The duration of the binary evolution captured by Figure 4 is 100 yr. Although the system can be rescaled to different masses, times, and separation, the initial separation in Figure 4 is $\sim 10^{-3} \text{ pc}$, when the binary enters its GW-dominated phase.

The increasing orbital speed of the binary leads to an increase in the jet’s precession angular velocity. This increases the helical winding of the jet such that the jet is wound up increasingly tightly closer to the source. This gives rise to a “chirping” morphology as seen in Figure 4. The chirp is easier to resolve in jets that are closer to the line of sight, where superluminal motion can magnify the forward jet. A chirping black hole is an unambiguous signature of a rapidly evolving binary BH system; the chirp is direct reflection of the orbital velocity evolution of the binary. Together, the three features of the jet morphology in Figure 4 are:

- Increase in the helical winding of the jet towards the central source (“chirpyness”),
- Widening of the opening angle towards the central source, and
- An apparent variation in the jet precession axis towards the central source (“twist”).

These directly probe the dynamics of the binary in its GW phase.

4.1 Can chirping jets be observed?

Observations of such a milliarcsecond scale geometry with the three features described above can thus flag a BH binary nearing the end of its merger. We now consider the question of whether such morphologies will be measurable in real observations.

As discussed in Section 1, several helical jets have been observed thanks to VLBI. A resolution of few tens of microarcseconds can be achieved using the Very Long Baseline Array (VLBA) with sensitivity of up to $30 \mu\text{Jy}/\text{beam}$, as demonstrated by the MOJAVE survey (Lister et al. 2009). VLA has angular resolution of few tens of milliarcseconds with a sensitivity of about $100 \mu\text{Jy}/\text{beam}$. The European VLBI network (EVN) which can resolve up to 0.13 milliarcseconds and can detect surface brightness down to $19 \mu\text{Jy}/\text{beam}$. The Very Large Array (VLA) has an angular resolution of few tens of milliarcseconds with a sensitivity of about $100 \mu\text{Jy}/\text{beam}$. The future Square Kilometer Array (SKA) on its own will have 2 milliarcsecond resolution at around 10 GHz, but SKA will be an order of magnitude more sensitive than current instruments with a sensitivity of about $50 \text{ nJy}/\text{beam}$. Thus angular resolution of tens to hundreds of microarcseconds and flux sensitivity of a few $\mu\text{Jy}/\text{beam}$ is achievable with current VLBI instruments.

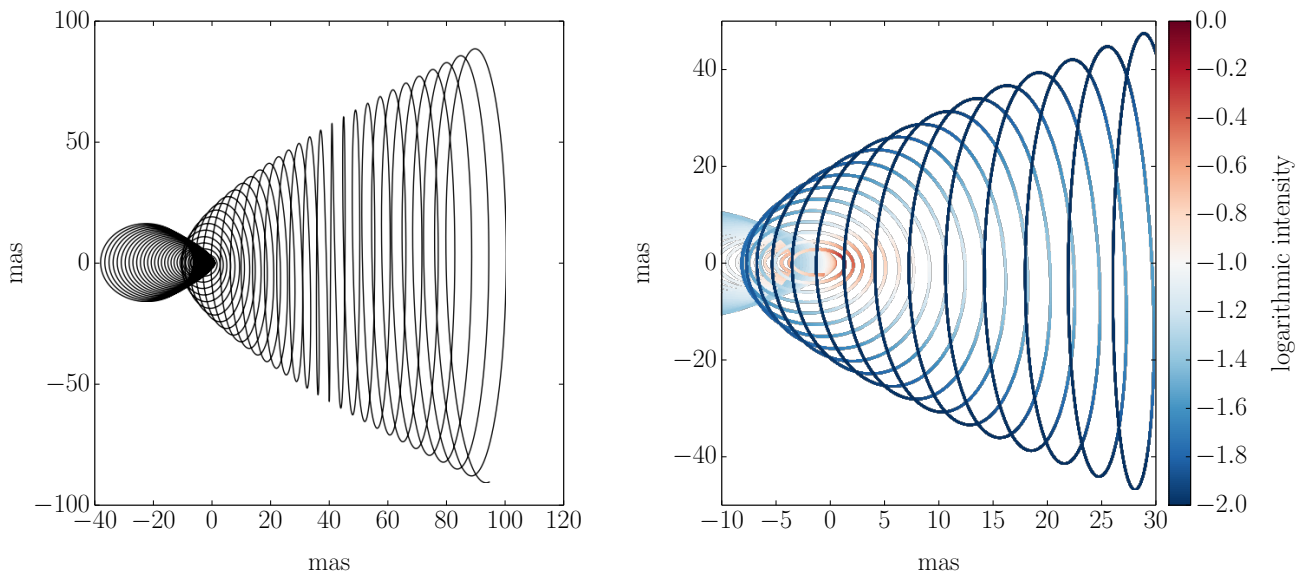


Figure 4. The left panel shows forward and backward jets for an equal-mass binary with total mass $M = 10^{10} M_{\odot}$. (This figure shows the position of many jet particles observed at a fixed time on Earth.) We have assumed $i = 40^{\circ}$, $\beta = 0.9$, and angular diameter distance $d = 100$ Mpc. The jets are twisted because of the apparent superluminal motion. Also evident is the opening of the jet and the radio jet chirp. Right panel shows normalised brightness of the inner 30 mas region of the forward jet. (This panel shows the intensity of many particles observed at a fixed time on Earth.)

The brighter part of the jet (intensity within factor of 10 from the maximum) in Figure 4 (right panel) has separations of ~ 1 mas. Figure 5 shows inner 100 square mas of the jet in Figure 4 smoothed at $200 \mu\text{as}$ and 2 mas respectively. We find that at $200 \mu\text{as}$ resolution the chirp is clearly resolved. At a lower resolution of 2 mas, the chirp is no longer resolved but widening of the jet opening angle can possibly be inferred. (In the next section, we discuss an algorithm to fit the jet model to observational data.) Note that other geometric effects can influence these conclusions. If it is aligned closer to the line of sight, the forward jet is magnified due to apparent superluminal motion. This will make it possible to resolve jets of objects that are farther away than the example in Figure 4. Binaries with higher masses have large orbital periods that will result in a helix with wider separation between its cycles. These objects would therefore be easier to detect. We have not modeled the absolute surface brightness of jets, only relative variation in the jet brightness (as shown in Figure 4), but due to the $(1+z)^{-4}$ dimming, it will be exceedingly difficult to detect such jets at higher redshifts.

We note here that there is at least one object in the literature that shows a jet morphology similar to Figure 4. The quasar 4C 18.68 described by Gower & Hutchings (1982a) shows a helical jet with an apparent opening angle that increases towards the central source from 11° to 45° in just two cycles (Gower et al. 1982). The observing beamwidth of about 400 mas makes it difficult to resolve a chirp in this source, but it is a prototype of the morphology that we are discussing here. Graham et al. (2015a) have reported that 111 candidates show periodic variability in brightness in the Catalina Real-time Transient Survey, indicating presence of binary BHs. An analysis of these candidates suggests the presence of circumbinary gas at small orbital distances

(Graham et al. 2015a). This bodes well for the likelihood of the presence of chirpy jets. In low resolution wide field surveys, detecting modulations in the light curves would be an easier diagnostic of a binary BH (O’Shaughnessy et al. 2011; Kaplan et al. 2011).

4.2 Deriving binary parameters from observations of chirping jets

From observations of chirping jets, we can infer the dynamical parameters of the binary BH by first fitting a purely geometric model to the observed jet morphology. To create a model of this kind, we generalise the simple helical model considered by Kun et al. (2014) and Nakamura et al. (2001) to write

$$z = x^{-\alpha} \frac{B}{2\pi} u \cos u, \quad (18)$$

$$y = x^{-\alpha} \frac{B}{2\pi} u \sin u, \quad (19)$$

$$x = \frac{A}{2\pi} u \left(\frac{u}{2\pi} \right)^{\beta}. \quad (20)$$

Here u is the azimuthal angle around the jet axis, x and y axes are in the plane of the sky, and the z axis points to the observer. The $x^{-\alpha}$ term in the first two equations captures the widening opening angle of the jet, while the $(u/2\pi)^{\beta}$ term in the last equation parameterises the chirp. This model can be fitted to an observed jet on the sky by using two rotation matrices, \mathcal{R}_{λ} and \mathcal{R}_i , which rotate the model in the above equations to match with the jet precession axis and the jet symmetry axis. These matrices are given by

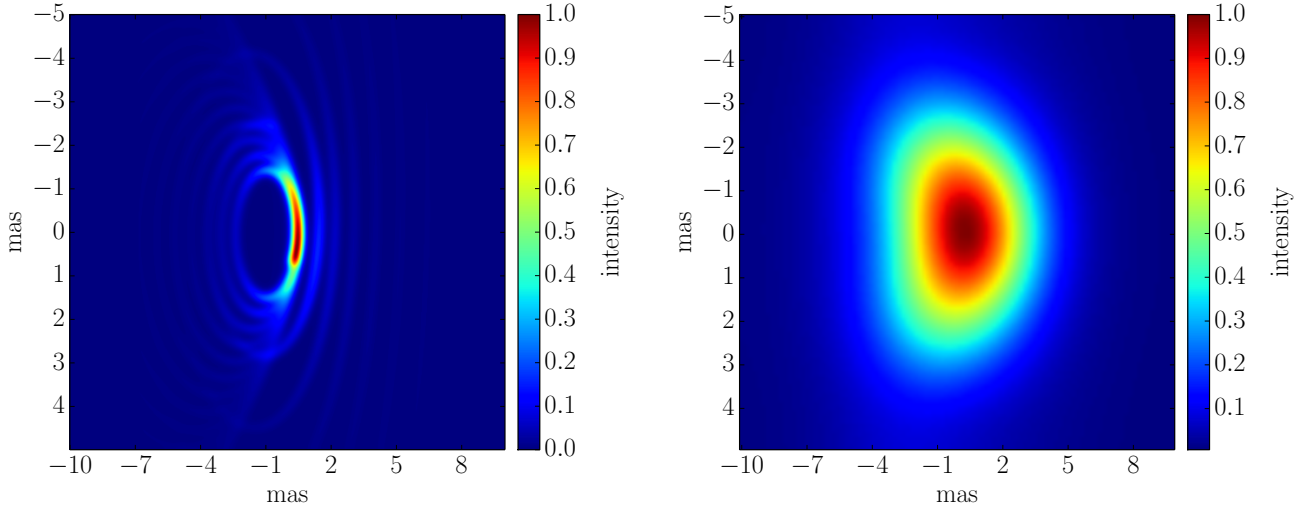


Figure 5. Central 100 square mas of the jet in Figure 4 smoothed at 200 μmas (left panel) and 2 mas (right panel) respectively. The intensity is normalised in arbitrary units.

$$R_i = \begin{pmatrix} \cos i & 0 & \sin i \\ 0 & 1 & 0 \\ -\sin i & 0 & \cos i \end{pmatrix} \quad (21)$$

and

$$R_\lambda = \begin{pmatrix} \cos \lambda_0 & -\sin \lambda_0 & 0 \\ \sin \lambda_0 & \cos \lambda_0 & 0 \\ 0 & 0 & 1 \end{pmatrix}. \quad (22)$$

Further, we can parameterise the “twist” in the jet by requiring that i and λ vary with x . Without loss of generality, we take this variation in i and parameterise it as

$$i = \gamma x + i_0. \quad (23)$$

We thus arrive at a model with 7 parameters (α , β , γ , A , B , i_0 , λ_0), which can be fitted to any observed jet, such as that in Figure 4. Note that setting α and β equal to 0 yields the usual helical jet morphology, without the features discussed in this paper. Thus, a non-zero value of these two parameters distinguishes chirpy jets from non-chirpy ones.

Figure 6 shows how the geometric model of this section works in practice, by fitting it to mock data using Markov Chain Monte Carlo (MCMC). We used the `emcee` package for this purpose (Foreman-Mackey et al. 2013). Mock data are created by using Equations (18)–(23) and then smoothing the resultant jet morphology by ~ 2 mas. Figure 6 shows posterior probability distributions of the parameters of our 7-parameter model when it is fit to these mock data. Wide, uniform priors were chosen for all parameters. The posteriors demonstrate that there is no degeneracy in the geometric model parameters. In fact the narrow ranges of values for which the posteriors are non-zero for each parameter show that the model fit the mock data very well.

The best fit geometric parameters can then be used to derive the dynamical parameters of the BH binary in the following way. The parameters α and B quantify the widening of the opening angle ψ . As each cycle of the observed helical jet corresponds to a period $P(t)$ of the binary, we can then write $d\psi/dP$, which yields a constraint on the quantity

a^4/M^3 as a function of P via Equations (2), (4) and (9). The parameters A and β , which quantify the chirp, can be used to directly infer the evolution of the binary separation as da/dP , which also constrains the quantity a^4/M^3 via Equation (4). These two constraints can be used to determine $a(P)$ and M separately. Finally, the parameters i_0 , λ_0 , and γ quantify the twist in the jet, which can potentially be used to constrain the quantity \dot{M} by using Equation (5).

Further parameters can be introduced in the dynamical model by considering unequal-mass binaries, eccentric orbits, and Post-Newtonian corrections, but we not develop this further in this paper. We make the code for implementing the model presented in this paper and for fitting it to observed jets using MCMC analyses available at <https://github.com/gkulkarni/JetMorphology> under the MIT open source software license. This code can be used to explore parameter space of the model.

5 CONCLUSION

Using a model of jet precession in a binary BH, we have shown that the jet produced by a member of a binary that is entering its GW-induced phase of inspiral exhibits a distinct chirping morphology. Jets in these binaries have a bi-conical morphology. After the binary enters the GW phase, the opening angle of cone rapidly increases within a separation of tens of milliarcseconds at a distance of ~ 100 Mpc, depending on the angle that the jet makes relative to the line of sight. In addition, the periodicity of the jet’s motion on the conical surface increases with the orbital period of the binary in this stage of its evolution. Finally, due to the apparent superluminal motion and the widening opening angle, the jet is twisted into a peculiar morphology. The jet geometry can be used to infer the set of dynamical and geometrical parameters.

Milliarcsecond features can be resolved using long baseline radio interferometry (Qian et al. 2001). At higher redshifts, jets are fainter and the wiggles become more difficult

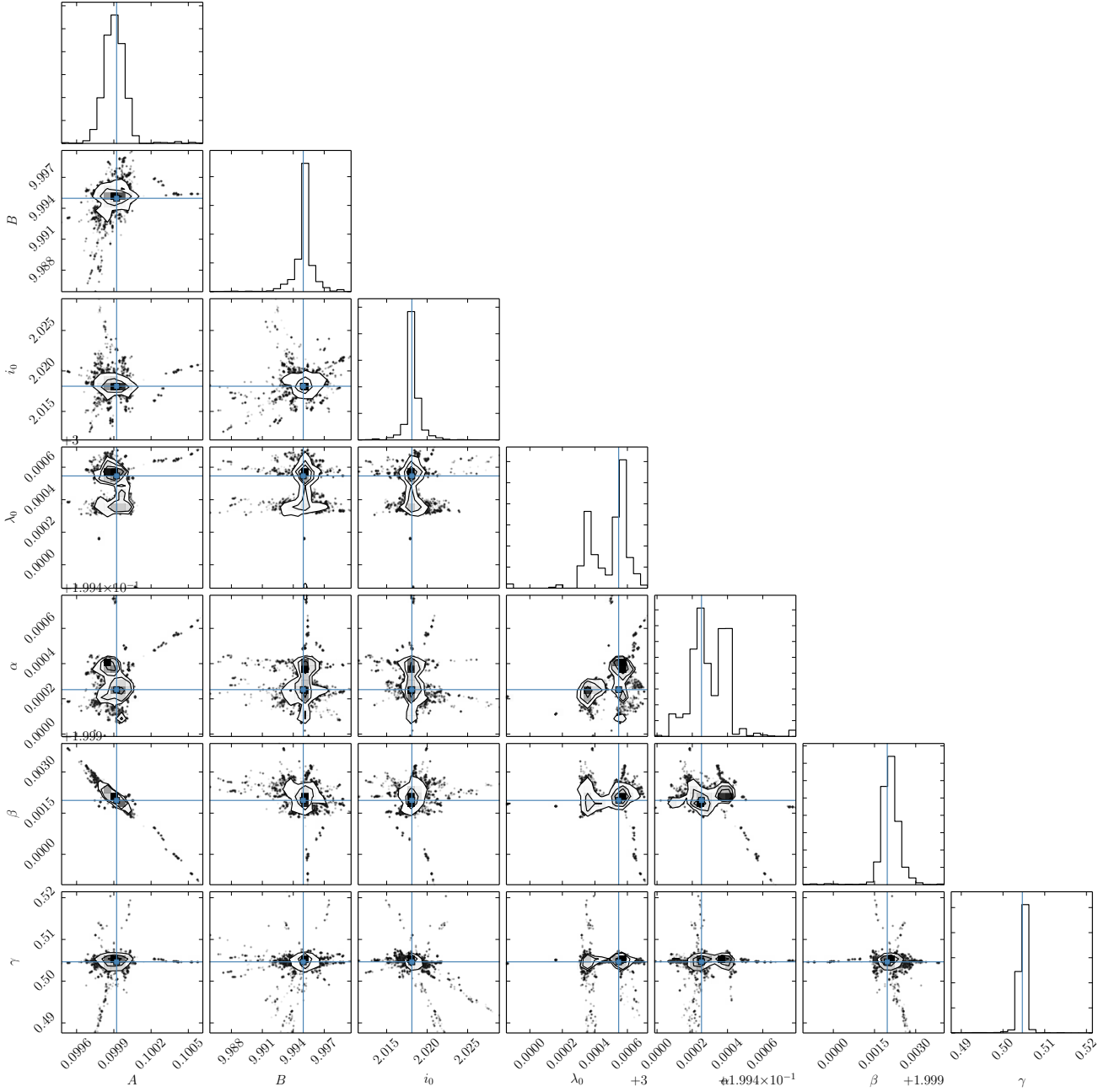


Figure 6. One and two dimensional projections of posterior probability distributions of the 7-parameter geometric model described in Section 4.2 to mock data. Wide, uniform priors were chosen for all parameters. The two-dimensional projections also show that there are no parameter degeneracies in the geometric model. As described in the text, these parameter values can then be used to derive various physical parameters describing the black hole binary.

to resolve. However, it might be possible to resolve binaries with very unequal mass ratios, eccentric orbits, or suitable inclinations. The future Square Kilometer Array (SKA) should make microarcsecond resolution possible, which could increase the detection rate of these objects (Paragi et al. 2015).

The jet morphology acts as an electromagnetic counterpart for chirping gravitational wave sources. BH binaries are expected to be the brightest GW sources in the universe.

Current ground based GW detectors such as LIGO are sensitive to intermediate-mass BH binaries at high redshift, which would be difficult to detect with our method. However, future detectors such as eLISA are sensitive to GW emission from 10^7 – 10^9 M_{\odot} BHs (Sesana 2013). Pulsar Timing Arrays are sensitive to even higher binary masses. Monitoring of jet morphologies for the features outlined in this paper will put a lower bound on the expected abundance of bright GW sources. Moreover, combined GW and electromagnetic

observations of compact binary mergers should enable detailed studies of astrophysical processes in the strong-field GR regime (Holz & Hughes 2005).

ACKNOWLEDGMENTS

We acknowledge helpful comments from the anonymous referee and useful discussions with Martin Haehnelt, Enrico Ramirez-Ruiz, and Alberto Rorai. This work was supported in part by NSF grant AST-1312034 (for A. L.) and by the FP7 ERC Advanced Grant Emergence-320596 (for G. K.).

REFERENCES

- Artymowicz P., Lubow S. H., 1994, *ApJ*, **421**, 651
- Baker J. G., Centrella J., Choi D.-I., Koppitz M., van Meter J., 2006, *Physical Review Letters*, **96**, 111102
- Begelman M. C., Blandford R. D., Rees M. J., 1980, *Nature*, **287**, 307
- Bode N., Phinney S., 2007, in APS April Meeting Abstracts. p. 1010
- Bon E., et al., 2012, *ApJ*, **759**, 118
- Britzen S., Roland J., Laskar J., Kokkotas K., Campbell R. M., Witzel A., 2001, *A&A*, **374**, 784
- Campanelli M., Lousto C. O., Marronetti P., Zlochower Y., 2006, *Physical Review Letters*, **96**, 111101
- Caproni A., Abraham Z., 2004, *MNRAS*, **349**, 1218
- Caproni A., Abraham Z., Monteiro H., 2013, *MNRAS*, **428**, 280
- Colpi M., Dotti M., 2011, *Advanced Science Letters*, **4**, 181
- Cuadra J., Armitage P. J., Alexander R. D., Begelman M. C., 2009, *MNRAS*, **393**, 1423
- D’Orazio D. J., Haiman Z., MacFadyen A., 2013, *MNRAS*, **436**, 2997
- Di Matteo T., Colberg J., Springel V., Hernquist L., Sijacki D., 2008, *ApJ*, **676**, 33
- Dotti M., Merloni A., Montuori C., 2015, *MNRAS*, **448**, 3603
- Farris B. D., Gold R., Paschalidis V., Etienne Z. B., Shapiro S. L., 2012, *Physical Review Letters*, **109**, 221102
- Farris B. D., Duffell P., MacFadyen A. I., Haiman Z., 2014, *ApJ*, **783**, 134
- Farris B. D., Duffell P., MacFadyen A. I., Haiman Z., 2015, *MNRAS*, **446**, L36
- Foreman-Mackey D., Hogg D. W., Lang D., Goodman J., 2013, *PASP*, **125**, 306
- Gold R., Paschalidis V., Etienne Z. B., Shapiro S. L., Pfeiffer H. P., 2014a, *Phys. Rev. D*, **89**, 064060
- Gold R., Paschalidis V., Ruiz M., Shapiro S. L., Etienne Z. B., Pfeiffer H. P., 2014b, *Phys. Rev. D*, **90**, 104030
- Gower A. C., Hutchings J. B., 1982a, *ApJ*, **253**, L1
- Gower A. C., Hutchings J. B., 1982b, *ApJ*, **258**, L63
- Gower A. C., Gregory P. C., Unruh W. G., Hutchings J. B., 1982, *ApJ*, **262**, 478
- Graham M. J., et al., 2015a, *MNRAS*, **453**, 1562
- Graham M. J., et al., 2015b, *Nature*, **518**, 74
- Haehnelt M. G., Kauffmann G., 2002, *MNRAS*, **336**, L61
- Haiman Z., Kocsis B., Menou K., Lippai Z., Frei Z., 2009, *Classical and Quantum Gravity*, **26**, 094032
- Hayasaki K., Mineshige S., Sudou H., 2007, *PASJ*, **59**, 427
- Hjellming R. M., Johnston K. J., 1981, *ApJ*, **246**, L141
- Holz D. E., Hughes S. A., 2005, *ApJ*, **629**, 15
- Hughes S. A., Holz D. E., 2003, *Classical and Quantum Gravity*, **20**, 65
- Icke V., 1981, *ApJ*, **246**, L65
- Kaplan D. L., O’Shaughnessy R., Sesana A., Volonteri M., 2011, *ApJ*, **734**, L37
- Kauffmann G., Haehnelt M., 2000, *MNRAS*, **311**, 576
- Kocsis B., Loeb A., 2008, *Physical Review Letters*, **101**, 041101
- Kocsis B., Haiman Z., Loeb A., 2012, *MNRAS*, **427**, 2680
- Kulkarni G., Loeb A., 2012, *MNRAS*, **422**, 1306
- Kun E., Gabányi K. É., Karouzos M., Britzen S., Gergely L. Á., 2014, *MNRAS*, **445**, 1370
- Kun E., Frey S., Gabányi K. É., Britzen S., Cseh D., Gergely L. Á., 2015, *MNRAS*, **454**, 1290
- Lippai Z., Frei Z., Haiman Z., 2008, *ApJ*, **676**, L5
- Lister M. L., et al., 2009, *AJ*, **138**, 1874
- Lobanov A. P., Roland J., 2005, *A&A*, **431**, 831
- Loeb A., 2007, *Physical Review Letters*, **99**, 041103
- Loeb A., 2010, *Phys. Rev. D*, **81**, 047503
- MacFadyen A. I., Milosavljević M., 2008, *ApJ*, **672**, 83
- McKernan B., Ford K. E. S., Kocsis B., Haiman Z., 2013, *MNRAS*, **432**, 1468
- Merritt D., Milosavljević M., 2005, *Living Reviews in Relativity*, **8**, 8
- Milosavljević M., Phinney E. S., 2005, *ApJ*, **622**, L93
- Nakamura M., Uchida Y., Hirose S., 2001, *New Astron.*, **6**, 61
- Noble S. C., Mundim B. C., Nakano H., Krolik J. H., Campanelli M., Zlochower Y., Yunes N., 2012, *ApJ*, **755**, 51
- O’Shaughnessy R., Kaplan D. L., Sesana A., Kamble A., 2011, *ApJ*, **743**, 136
- Paragi Z., et al., 2015, Advancing Astrophysics with the Square Kilometre Array (AASKA14), p. 143
- Peters P. C., 1964, *Physical Review*, **136**, 1224
- Pretorius F., 2005, *Physical Review Letters*, **95**, 121101
- Qian S.-J., et al., 2001, *Chinese J. Astron. Astrophys.*, **1**, 236
- Roedig C., Sesana A., Dotti M., Cuadra J., Amaro-Seoane P., Haardt F., 2012, *A&A*, **545**, A127
- Roland J., Britzen S., Kudryavtseva N. A., Witzel A., Karouzos M., 2008, *A&A*, **483**, 125
- Romero G. E., Chajet L., Abraham Z., Fan J. H., 2000, *A&A*, **360**, 57
- Roos N., Kaastra J. S., Hummel C. A., 1993, *ApJ*, **409**, 130
- Sarazin C. L., Begelman M. C., Hatchett S. P., 1980, *ApJ*, **238**, L129
- Sesana A., 2013, *Classical and Quantum Gravity*, **30**, 244009
- Shapiro S. L., 2010, *Phys. Rev. D*, **81**, 024019
- Shi J.-M., Krolik J. H., 2015, *ApJ*, **807**, 131
- Shields G. A., Bonning E. W., 2008, *ApJ*, **682**, 758
- Stirling A. M., et al., 2003, *MNRAS*, **341**, 405
- Stone N., Loeb A., 2011, *MNRAS*, **412**, 75
- Tanaka T., Menou K., 2010, *ApJ*, **714**, 404
- Valtonen M. J., Wiik K., 2012, *MNRAS*, **421**, 1861
- Villata M., Raiteri C. M., 1999, *A&A*, **347**, 30

This paper has been typeset from a $\text{\TeX}/\text{\LaTeX}$ file prepared by the author.